FULL WAVEFORM INVERSION OF REFLECTED SEISMIC DATA

SHENG XU[1*], FENG CHEN[1**], GILLES LAMBARÉ[2] and YU ZHANG[3]

[1] *CGG, 10300 Town Park Drive, Houston, TX 77072, U.S.A.*
[2] *CGG, 27 avenue Carnot, 91341 Massy-Cedex, France. gilles.lambare@cgg.com*
[3] *CGG, Crompton Way Manor Royal Estate, RH10 9QN Crawley, U.K. yu.zhang@cgg.com*
* *Present address: Statoil, 2103 Citywest Blvd., Houston, TX 77042, U.S.A. SXU@statoil.com*
** *Present address: Conoco Phillips, 600 N. Dairy Ashford, Houston, TX 77079, U.S.A. feng.chen@cop.com*

(Received February 26, 2013; revised version accepted July 29, 2013)

ABSTRACT

Xu, S., Chen, F., Lambaré, G. and Zhang, Y., 2013. Full waveform inversion of reflected seismic data. *Journal of Seismic Exploration*, 22: 449-462.

Full waveform inversion has been widely used to build shallow high resolution velocity models. Successful inversion requires seismic data with reliable refracted waves and low frequencies. In this paper, we revisit full waveform inversion theory and highlight a method to relax the dependence of inversion on low frequency reflections. The method can update the long wavelength components of the velocity model by using the reflected arrivals, even when the low frequency components of seismic data are absent in the input. Our approach involves a non-linear iterative relaxation approach where short and long wavelength components of the velocity model are updated alternatively. The approach still targets at matching observed data with simulated data, except the later are computed through a demigration process using the migrated images as reflectivity model. The overall workflow for the inversion in this paper is similar to the algorithm of migration based travel time waveform inversion proposed by Chavent et al. (1994) (the short wave length components of the velocity models are just replaced by a reflectivity distribution). We derive the inversion equations using Born's approximation and numerically analyze the Fréchet derivatives of the inversion. As a result we propose an efficient methodology taken advantage of the know how about preserved amplitude migration. At the end, we present a preliminary 2D application to a Gulf of Mexico conventional streamer dataset.

KEY WORDS: imaging, full waveform inversion, reflection, velocity.

0963-0651/13/$5.00

INTRODUCTION

In complex areas, there are two main challenges in prestack depth imaging: velocity model building and depth migration. Velocity model building estimates a velocity model for the simulation of seismic wave propagation that takes place during depth migration. This velocity model should contain the long wavelength (macro) components of the Earth model, while the depth migrated image should provide the short wavelength (reflectivity) details. So far seismic ray-based tomography (Bishop et al., 1985; Liu and Bleistein, 1995; Billette and Lambaré, 1998; Zhou et al., 2003; Woodward et al., 2008; Lambaré, 2008) has been widely used for velocity model building. However, the accuracy of these methods highly depends on the picking of events, which is a tedious and labour intensive task and is difficult to be fully automated when signal to noise ratio in the seismic is low (Siliqi et al., 2007; Liu and Han, 2010).

There has been a lot of effort to improve the resolution of ray-based tomography (Guillaume et al., 2011; Hu and Zhou, 2011), but geophysicists now also expect a wave equation based approach which would automatically invert a high resolution velocity where ray tracing fails to work properly. Full waveform inversion (FWI) aims at achieving this, and it has been demonstrated that FWI works on real data in different geological scenarios (Tarantola, 1984; Sirgue and Pratt, 2004; Virieux and Operto, 2009).

Classical FWI involves the least squares minimization of the misfit function between the simulated and observed data. Non-linear gradient based optimizations are used (Pratt et al., 1998; Ravaut et al., 2004; Sirgue and Pratt, 2004; Choi et al., 2008; Ma and Hale, 2011; Choi and Alkhalifah, 2011) with complex strategies to regularize the process (filtering, weighting and muting the data, etc. ...). Classical FWI theory requires fitting seismic waves in both amplitude and phase. Fitting the amplitude is difficult and may lead the velocity inversion to a wrong convergence, as amplitudes are sensitive to numerous complex parameters (anisotropy, elasticity, porosity, viscosity, source radiation pattern, attenuation, density model, etc. ...) which are difficult to be determined from the analysis of seismic data. Thus FWI based on the phase information appears more attractive and natural, and has been investigated (Luo and Schuster, 1991; Zhang et al., 2011). All these strategies mitigate non-linearity but cannot recover the features that are not covered by the intrinsic resolution of the method.

The resolution of FWI is the resolution of a migration operator (Lailly, 1983; Tarantola, 1984). The recovered wavelengths in the velocity model correspond to the recorded temporal period stretched to depth according to the local velocity and angular aperture. For the transmissions and refractions, the stretching due to the angle aperture allows us to recover the long wavelengths of the velocity model (Gauthier et al., 1986), while for the reflected seismic

waves, only short wavelengths can be recovered by FWI due to the narrow range of reflection angle apertures. This explains why FWI recovers long wavelength components of the velocity model only in shallow areas and why its resolution improves when lower frequencies and longer offset data are available (Ravaut et al., 2004; Sirgue et al., 2010). Unfortunately, for conventional streamer data, extremely low frequencies (less than 2 Hz) are not available due to the existence of the source and receiver ghost (Lindsey, 1960), while the available low frequency components of the data (2-5 Hz) exhibit poor signal-to-noise ratio. The maximum offset is usually around 8 $\sim$ 10 km, which limits the penetration depth of seismic diving waves. Application of FWI to streamer data then definitely remains a challenge (Plessix and Rynja, 2010).

There are some other difficulties related to the accuracy of FWI algorithm. For example, conventional FWI requires an accurate estimation of source signature, which may bring difficulties for real data application, especially for the algorithms in time domain. Moreover to compute the amplitude of the wave correctly, FWI requires a density model which is unknown for real cases, while simultaneously inverting for density and velocity models brings more ambiguities in the inversion problem (Virieux and Operto, 2009).

In this context alternative approaches for FWI have been proposed. While the cost function is in the recorded data domain for classical FWI (Tarantola, 1984; Sirgue and Pratt, 2004; Virieux and Operto, 2009), some FWI approaches work in the prestack depth migrated domain or in some other favourable domains (Zhang and Wang, 2009). Among the methods working in the depth migrated domain, wave-equation based tomography replaces the data matching objective function by a focusing criterion on either common image gathers or at the back propagated shot locations (Sava et al., 2005; Albertin et al., 2006; Soubaras and Gratacos, 2007; Shen and Symes, 2008; Albertin, 2011). Such methods have strong connections with conventional ray based migration velocity analysis (Woodward et al., 2008) and may suffer from the various artefacts encountered in depth migrated gathers.

We propose an alternative approach. Our cost function is based on the residual between the simulated and observed data as in classical full waveform inversion (FWI) but is now minimized with an iterative relaxation approach where the velocity model is split into long and short wavelength components, i.e., the background and the perturbation models. Inside each loop, first, the short wavelength components of the velocity model are obtained from the initial background model by a true amplitude migration; then this perturbation is fixed and the background model is updated by a local optimization scheme. We show in this article the expression of the associated Fréchet derivatives and gradients of the cost function, and discuss how and why such a strategy greatly improves the resolution we expect from FWI. Finally we present an application of our

algorithm to a 2D Gulf of Mexico streamer dataset, showing that the approach can update long wavelength components of the velocity model in a real case.

FRÉCHET DERIVATIVES AND GRADIENT OF THE COST FUNCTION FOR FWI

Let's start from the scalar acoustic wave equation. In the frequency domain the associated Green's function $G(\mathbf{x},\omega,\mathbf{s})$ (where $\mathbf{x}$ is spatial location, ω is the angular time frequency, and $\mathbf{s}$ is the shot position) satisfies the equation

$$-\omega^2 m(\mathbf{x})G - \nabla^2 G = \delta(\mathbf{x} - \mathbf{s}) \quad , \tag{1}$$

where $m(\mathbf{x}) = 1/v^2(\mathbf{x})$ is the model to be estimated, i.e., the square of the slowness. The traditional full waveform inversion uses a least square cost function

$$C(m) = \tfrac{1}{2} \int\int\int d\mathbf{s}d\mathbf{r}d\omega \, \| G_{obs} - G_{cal}(m) \|^2 \quad , \tag{2}$$

where $G_{obs}(\mathbf{r},\omega,\mathbf{s})$ and $G_{cal}(\mathbf{r},\omega,\mathbf{s})$ denote the observed and calculated Green's functions at the source and receiver positions ($\mathbf{s}$ and $\mathbf{r}$), respectively. Let's decompose the model into

$$m = m_0 + \delta m \quad , \tag{3}$$

where m_0 denotes a background model containing the long wavelength components of the velocity model, which determines the transmission behavior of the wave, and where δm denotes the perturbation model containing the short wavelength components of the velocity model, which determines the reflection behavior of the wave. Accordingly the Green's functions can also be decomposed into

$$G = G_0 + \delta G \, ., \tag{4}$$

An exact expression of the perturbation of the Green's function δG depending on m_0 and δm is given by the following Fredholm integral equation of the second kind (Polyanin and Manzhirov, 1998),

$$\delta G(m_0,\delta m)(\mathbf{r},\mathbf{s}) = \omega^2 \int d\mathbf{x} G_0(\mathbf{r},\mathbf{x}) G(\mathbf{x},\mathbf{s}) \delta m(\mathbf{x}) \quad , \tag{5}$$

where we have omitted dependency of ω in the expressions of the Green's functions. We see the symmetry of the expression (5) with respect to m_0 and $m_0+\delta m$, or, alternatively to $m-\delta m$ and m. It is interesting now to investigate the Fréchet derivatives of δG with respect to δ and m_0. Eq. (5) is not suitable

for numerical computation using direct integral, because it contains the unknown term $G(\mathbf{x},\mathbf{s})$ on the right hand side. Within the first order Born approximation, the perturbation Green's function can be easily computed by the integral

$$\delta G^{Born}(m_0,\delta m)(\mathbf{r},\mathbf{s}) \approx \omega^2 \int d\mathbf{x} G_0(\mathbf{r},\mathbf{x}) G_0(\mathbf{x},\mathbf{s}) \delta m(\mathbf{x}) \quad , \tag{6}$$

where we have broken the symmetry of the former eq. (5) by choosing the Green's functions in the background model m_0 rather than in the model m. The expression of the Fréchet derivative of G with respect to δm is the conventional kernel of the Born operator, i.e.,

$$\partial G^{Born}(\mathbf{r},\mathbf{s})/\partial \delta m(\mathbf{x}) = \omega^2 G_0(\mathbf{r},\mathbf{x}) G_0(\mathbf{x},\mathbf{s}) \quad . \tag{7}$$

It depends on m_0 but not on δm, and corresponds to the Fréchet derivative of the conventional full waveform inversion problem. As such it is also the kernel of a "normal" migration operator (Lailly, 1983; Tarantola, 1984).

The gradient of the cost function (2) can be easily computed from the Fréchet derivative as

$$\partial C/\partial \delta m(\mathbf{x}) =$$

$$-\omega^2 \int\int d\mathbf{r} d\mathbf{s} \int d\omega \mathrm{Re}\{G_0^*(\mathbf{r},\mathbf{x}) G_0^*(\mathbf{x},\mathbf{s}) [G_{obs}(\mathbf{r},\mathbf{s}) G_0(\mathbf{r},\mathbf{s})]\} \quad , \tag{8}$$

where the superscript * denotes the complex conjugate, and Re() denotes the real part of the complex function. In theory, the Green's function contains all the waves: direct arrivals, refractions and scattered waves, etc. However, with a smooth initial model, the calculated Green's function is dominated by the direct arrivals and diving waves. Their contribution to the gradient function of FWI is illustrated in Fig. 1a, while the contribution of the reflections is the "normal" migration response of the residuals, as shown in Fig. 1b. We see that FWI can potentially recover the long wavelength components of the velocity model in the shallow area (in fact along the diving wave paths) (Thanks to reflections it can also recover the short wave-length parts of the velocity model, e.g., by finding detailed channel systems). However, it is difficult to recover the long wavelength components of the velocity in the deeper area if sufficiently low frequencies are not present in the data (Plessix et al., 2010).

Following Chavent et al. (1994), let's now have a look at the Fréchet derivative of the cost function (2) with respect to the background model, m_0. Note that having chosen in the Born approximation the Green's functions in the background model m_0 (rather than those in the model m), we have removed the symmetry we pointed out in Fredholm eq. (5). From eq. (6), we have the expression:

$$\partial\delta G(\mathbf{s},\mathbf{r})/\partial m_0(\mathbf{y}) = \omega^2 \int d\mathbf{x}\delta m(\mathbf{x})\{[\partial G_0(\mathbf{s},\mathbf{x})/\partial m_0(\mathbf{y})]G_0(\mathbf{x},\mathbf{r}) + G_0(\mathbf{s},\mathbf{x})[\partial G_0(\mathbf{x},\mathbf{r})/\partial m_0(\mathbf{y})]\} \quad . \tag{9}$$

Then using the fact that

$$\partial G_0^{Born}(\mathbf{s},\mathbf{r})/\partial m_0(\mathbf{y}) = \omega^2 G_0(\mathbf{s},\mathbf{y})G_0(\mathbf{y},\mathbf{r}) \quad , \tag{10}$$

we obtain for (9)

$$\partial\delta G(\mathbf{s},\mathbf{r})/\partial m_0(\mathbf{y}) = \omega^4 \int d\mathbf{x}\delta m(\mathbf{x})[G_0(\mathbf{s},\mathbf{y})G_0(\mathbf{y},\mathbf{x})G_0(\mathbf{x},\mathbf{r}) + G_0(\mathbf{s},\mathbf{x})G_0(\mathbf{x},\mathbf{y})G_0(\mathbf{y},\mathbf{r})] \quad , \tag{11}$$

where we can recognize Born approximation (6) and obtain approximation

$$\partial\delta G(\mathbf{s},\mathbf{r})/\partial m_0(\mathbf{y}) = \omega^2[G_0(\mathbf{s},\mathbf{y})\delta G^{Born}(\mathbf{y},\mathbf{r}) + \delta G^{Born}(\mathbf{s},\mathbf{y})G_0(\mathbf{y},\mathbf{r})] \quad . \tag{12}$$

This expression applies the first order approximation of the perturbed wavefield δG^{Born} over all the propagation medium (parameterized by $\mathbf{y}$) for shot and receiver positions $\mathbf{s}$ and $\mathbf{r}$. This approximated perturbed wavefield can be obtained by a forward Born modeling equivalent to what we call a demigration process (the short wavelength component of the velocity model are then replaced by a reflectivity distribution).

Finally we obtain for the gradient of the cost function [eq. (9)] with respect to m_0 (fixing δm) the expression

$$\partial C/\partial m_0(\mathbf{y})\big|_{\delta m} \approx - \iint d\mathbf{r}d\mathbf{s} \int d\omega\{\partial\delta G^*(\mathbf{r},\mathbf{s})/\partial m_0(\mathbf{x})\big|_{\delta m} \times [G_{obs}(\mathbf{r},\mathbf{s}) - G_0(\mathbf{r},\mathbf{s})]\} \quad . \tag{13}$$

We can analyze the contribution of the reflected waves to this gradient of the cost function. We see on Figs. 1c and 1d, that the contribution to the gradient of the reflected waves is now spread along the wave propagation paths of the reflections (Figs. 1c and 1d). Fig. 1c shows the contribution corresponding to the wave path from the source to the reflector [the first term on the right hand side of eq. (12)] while Fig. 1d shows the total contribution, source-reflector-receiver. We now observe that a local optimization of C for m_0 (fixing δm at each non-linear iteration) may be suitable for recovering the long wavelength components in depth of the velocity model available in the reflections. As noticed by Chavent et al. (1994) we have here the framework for developing a full waveform inversion approach capable of recovering long

wavelengths of the velocity model from reflected arrival even in the deep parts of the models.

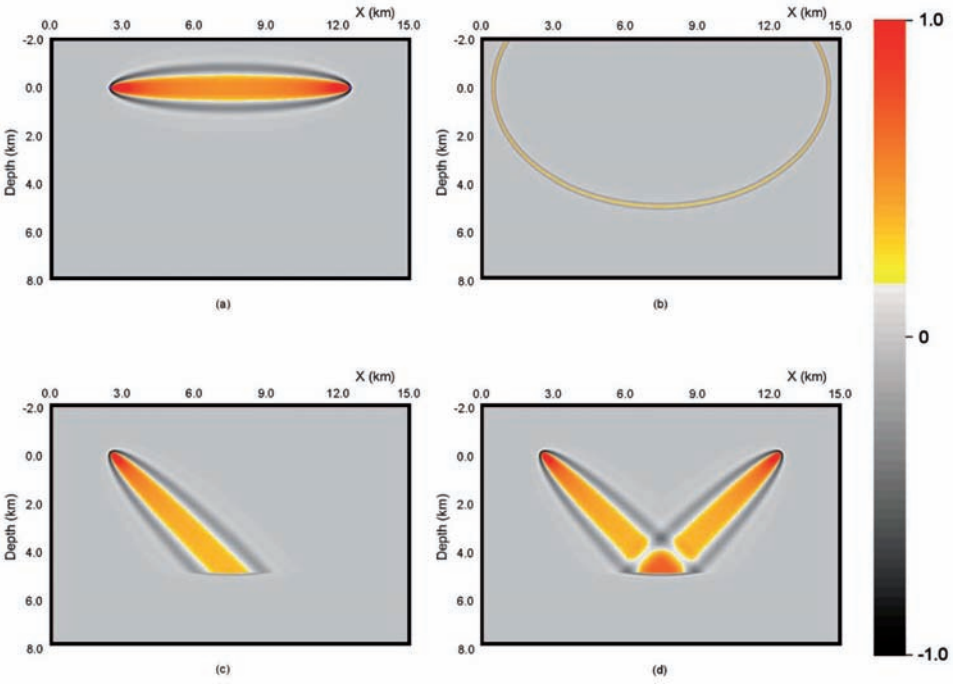

Fig. 1. Contribution to the gradients of classical FWI and SRFWI [eqs. (7) and (10)] of a trace with the source location at (2.5, 0.0) km, and receiver location at (12.5, 0.0) km. The source wavelet is a Ricker with a peak frequency at 6.0 Hz; and the background velocity is 2.0 km/s. Two signals are considered as residuals: a direct wave and a reflected wave for a reflector at 5 km depth.
a) Contribution of the direct wave to the gradient of classical FWI; b) Contribution of the reflected wave to the gradient of classical FWI; c) Source-reflector contribution of the reflected wave to the gradient of SRFWI; d) Source-reflector-receiver contribution of the reflected wave to the gradient of SRFWI.

REFLECTED SEISMIC FULL WAVEFORM INVERSION

Based on the discussion of previous section, we propose an approach where background m_0 is iteratively updated through a non-linear local optimization scheme. Starting from an initial background velocity model m_0, in expression (9) the term δG^{Born} is approximated by a wave equation modelling using the model and the reflectivity derived from the true amplitude migration (Bleistein, 1987; Zhang et al., 2007; Zhang et al. 2013). Each iteration consists

of the following steps:

1. Apply a true amplitude prestack depth migration to the reflected wavefield using the initial background model m_0^{init} (Zhang et al., 2013) and generate the migration image δm;

2. Use prestack demigration [eq. (6)] to generate the synthetic wave field δG_{cal} with the initial background velocity model m_0^{init} and the image δm from step 1;

3. Compute the residual data to obtain the cost function;

4. Compute the gradient of the cost function using eqs. (12) and (13);

5. Update the background velocity model to $m_0^{updated}$;

6. Go to the next iteration or terminate.

In step 1, we decompose local wave field in angle domain and only stack the near angle image to output δm (Xu et al., 2011). The reason of not using the full stacked image is that when the initial background velocity is far from the real one, the full stacked image cannot focus well and this will alter the quality of data obtained by demigration. On the other hand, if we stick to the near angle/offset reflections, demigrate following by a migration should recover the kinematics and easily match the input data. Therefore, we started with δm generated by a partially stacked near angle image (e.g., 0 ~ 20 degrees), then with the improved updated background velocity model obtained at each iteration, we gradually increase the stacked angle range of the migrated image to 0 ~ 45 degrees. By doing this, we reduce the cycle-skip problem and relax the low frequency requirement for the inversion.

Note that we approximate the wavefield δG^{Born} by a demigration process taking the reflectivity function obtained from true amplitude migration rather than the velocity perturbation obtained from preserved amplitude migration (Beylkin, 1985; Operto et al., 2000; Xu et al., 2001). In order to focus on the reflected wavefield, the direct arrivals and refractions are muted in δG. The relaxation approach proposed here is the same as the one used in the migration-based travel time tomography (MBTT) approach proposed by Chavent et al. (1994) or Clément et al. (2001), or its alternative ray-based implementation, for example, Plessix et al. (1999). As it is a full waveform inversion method, we prefer to call it Seismic Reflection Full Waveform Inversion (SRFWI). Note that it has also some similarity in terms of resolution with the differential semblance optimization (DSO) method proposed by Symes and Carazzone (1991).

APPLICATION

We apply our 2D reflected seismic FWI algorithm to a dataset from Mississippi Canyon in Gulf of Mexico. A 2D line was extracted from a 3D narrow azimuth streamer dataset. The target is the velocity anomaly associated to a gas cloud. To ensure the efficiency, we equally decimated 2/3 of the shots and the shot spacing used in the inversion is 738 feet. The input data has been low pass-filtered down to 12 Hz. The initial background velocity model (Fig. 2) is obtained from a high resolution ray based tomography (Han and Xu, 2011). It takes non-linear 13 iterations to obtain the final background velocity model shown on Fig. 3. The final velocity perturbation is shown in Fig. 4. Since the data is from a conventional narrow azimuth acquisition, it does not contain much signal below 5 Hz. Note that the acquired maximum offset is approximately 8 km and that the water bottom is about 1 km deep. It would be hard for a conventional FWI to produce for this dataset a velocity perturbation with long wavelength components. However, as shown in Fig. 4, Seismic Reflection FWI clearly provides an update with long wavelength components down to 15000 feet in depth. Fig. 5 is the reverse time migration (RTM) image obtained for the initial background velocity model, while Fig. 6 shows the RTM image obtained for the updated background velocity model. We can observe the improved focusing of the seismic events, especially on the dipping events in the centre of images. Fig. 7 shows the RTM angle gathers (Xu et al., 2011) obtained for the initial background velocity model (Angles are between 0 and 60 degrees). Curving down events can be clearly observed in the common image gathers for most of the far angles. Fig. 8 shows the corresponding angle gathers obtained for the updated background velocity model. With the updated background velocity model the angle gathers are more flat, and the migrated stack is improved.

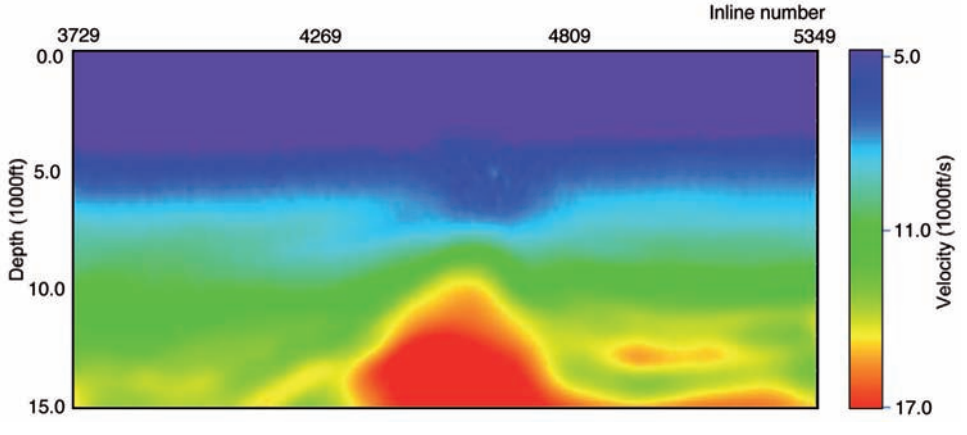

Fig. 2. Initial background velocity model.

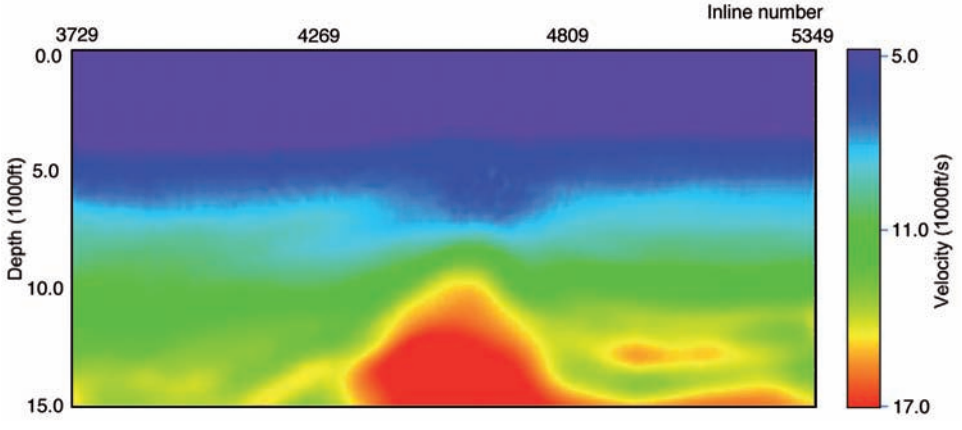

Fig. 3. Final updated background velocity model obtained by seismic reflection full waveform inversion.

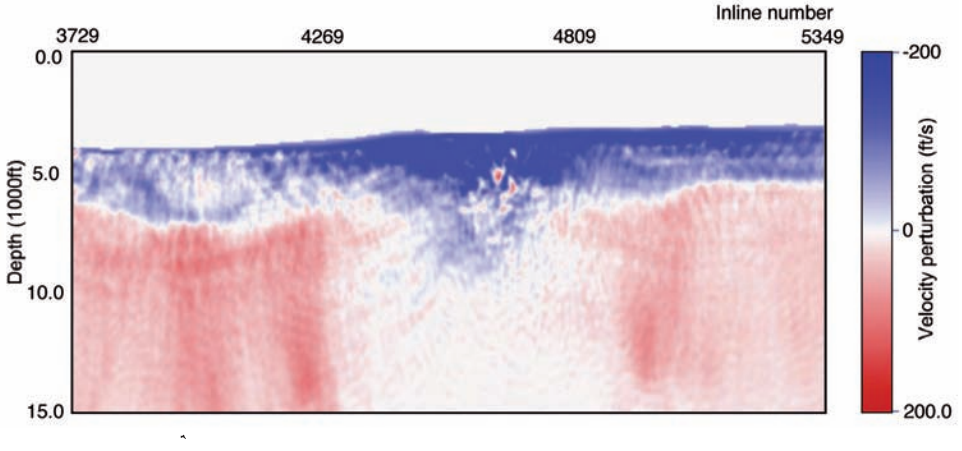

Fig. 4. Velocity updates obtained by seismic reflection full waveform inversion.

CONCLUSION

Following the approach proposed by Chavent et al. (1994) we have investigated a full waveform inversion approach where the long and short wavelength components of the velocity model are inverted iteratively by a relaxation approach. For each iteration, the short wavelength components are first inverted by true amplitude migration and then fixed and used to update the

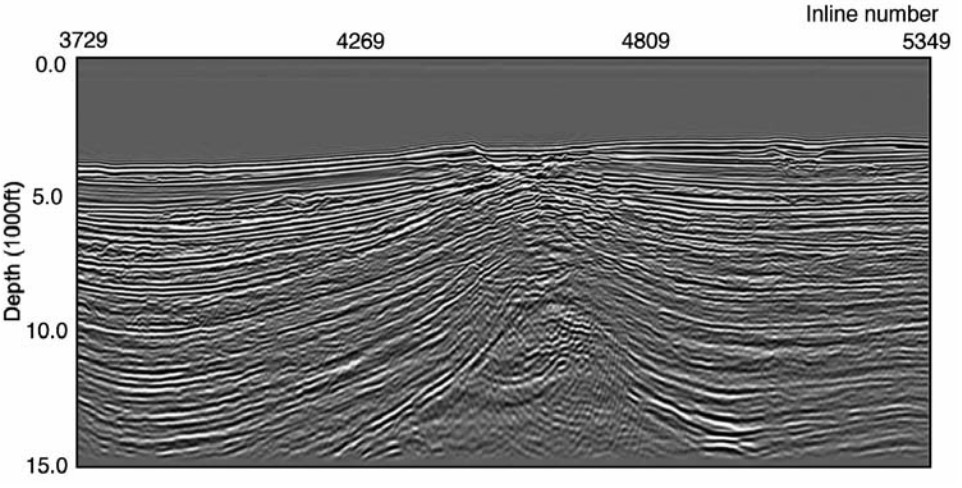

Fig. 5. RTM images obtained with the initial background velocity model.

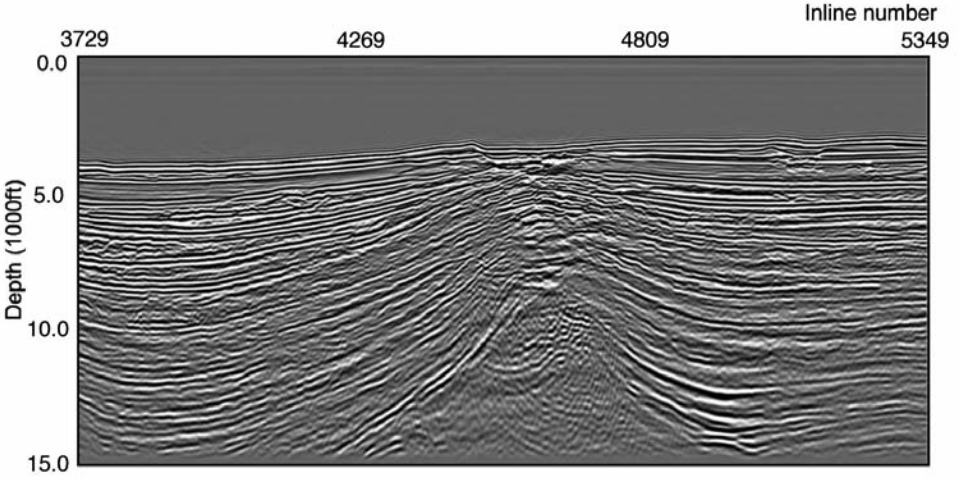

Fig. 6. RTM images obtained with the final updated background velocity model.

long wavelength components. The analysis of the resulting gradient shows the ability of the approach to update long wavelength components of the velocity along the reflected wave-path. This relaxation approach greatly enlarge the ability of full waveform inversion for velocity model building from reflectedwaves even when low frequency are not available in the input data. An application to a 2D real data example demonstrates that the proposed method works on conventional streamer data.

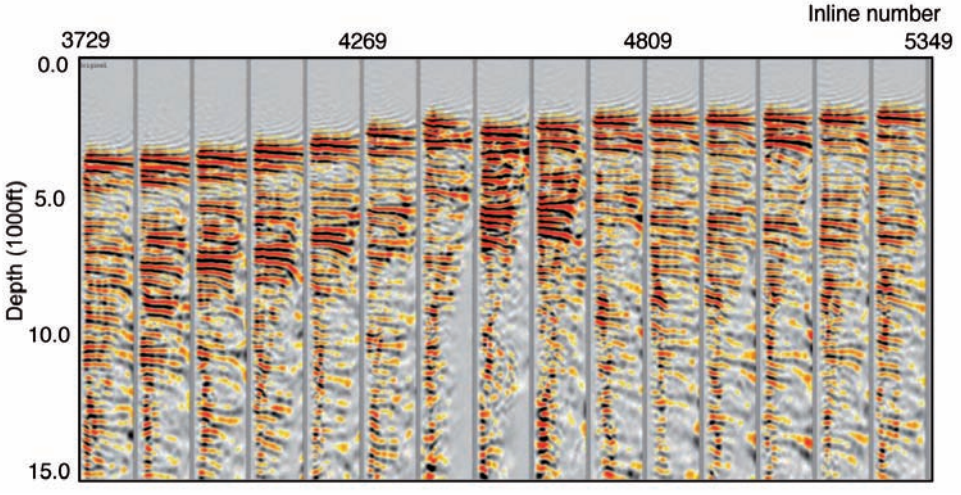

Fig. 7. RTM angle gathers obtained with the initial background velocity model.

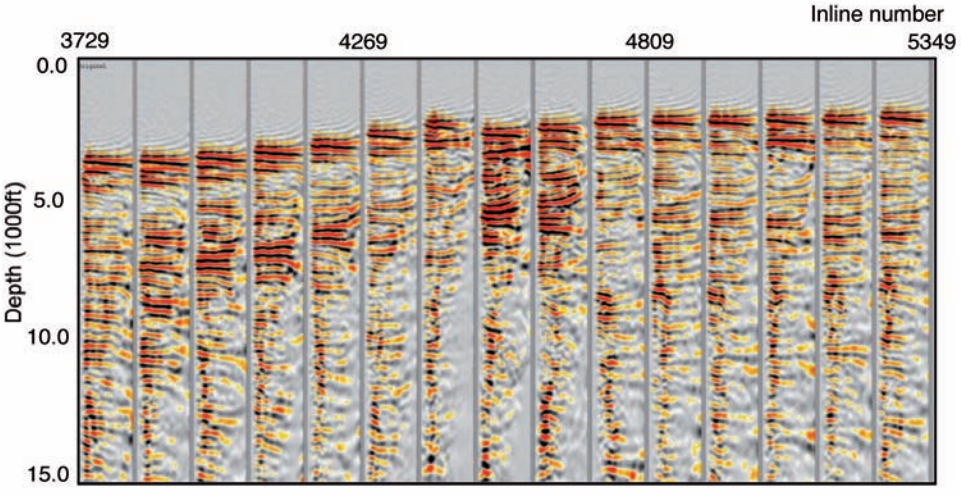

Fig. 8. RTM angle gathers obtained with the updated background velocity model.

ACKNOWLEDGEMENT

We thank CGG for the permission to publish this work. We thank Kristin Johnston for editing the paper, Patrice Guillaume and Vetle Vinje for reviewing the paper and Wim Mulder and René-Edouard Plessix (Shell) for helpful discussions.

REFERENCES

Albertin, U., Sava, P., Etgen, J. and Maharramov, M., 2006. Adjoint wave-equation velocity analysis. Expanded Abstr., 76th Ann. Internat. SEG Mtg., New Orleans: 3345-3349.

Albertin, U., 2011. An improved gradient computation for adjoint wave-equation reflection tomography. Expanded Abstr., 81st Ann. Internat. SEG Mtg., San Antonio: 3969-3973.

Beylkin, G., 1985. Imaging of discontinuities in the inverse scattering problem by inversion of a causal generalized Radon transform. J. Math. Phys., 26: 99-108.

Billette, F. and Lambaré, G., 1998. Velocity macro-model estimation from seismic reflection data by stereotomography. Geophys. J. Internat., 135: 671-680.

Bishop, T.N., Bube, K.P., Cutler, R.T., Langan, R.T., Love, P.L., Resnick, T.R., Shuey, R.T., Spinder, D.A. and Wyld, H.W., 1985. Tomographic determination of velocity and depth in laterally varying media. Geophysics, 50: 903-923.

Bleistein, N., 1987. On the imaging of reflectors in the Earth. Geophysics, 52: 931-942.

Chavent, G., Clément, F. and Gómez, S., 1994. Automatic determination of velocities via migration-based traveltime waveform inversion: A synthetic data example. Expanded Abstr., 64th Ann. Internat. SEG Mtg., Los Angeles: 1179-1182.

Choi, Y. and Alkhalifah, T., 2011. Application of encoded multi-source waveform inversion to marine-streamer acquisition based on the global correlation. Extended Abstr., 73rd EAGE Conf., Vienna: F026.

Choi, Y., Min, D.J. and Shin, C., 2008. Frequency-domain full waveform inversion using the new pseudo-Hessian matrix: Experience of elastic Marmousi-2 synthetic data. Bull. Seismol. Soc. Am., 98: 2402-2415.

Clément, F., Chavent, G. and Gómez, S., 2001. Migration-based traveltime waveform inversion of 2D simple structures: A synthetic example. Geophysics, 66: 845-860.

Gauthier, O., Virieux, J. and Tarantola, A., 1986. Two-dimensional nonlinear inversion of seismic waveforms: Numerical results. Geophysics, 51: 1387-1403.

Guillaume, P., Lambaré, G., Sioni, S., Carotti, D., Depr, P., Culianez, G., Montel, J.P., Mitouard, P., Depagne, S., Frehers, S. and Vosberg, H., 2011. Geologically consistent velocities obtained by high definition tomography. Expanded Abstr., 81st Ann. Internat. SEG Mtg., San Antonio: 4061-4065.

Han, W., Xu, S., 2011. High resolution velocity model for imaging complex structures. Extended Abstr., 73rd EAGE Conf., Vienna: B010.

Hu, L. and Zhou, J., 2011. Velocity update using high resolution tomography in Santos Basin, Brazil. Expanded Abstr., 81st Ann. Internat. SEG Mtg., San Antonio: 3974-3978.

Lailly, P., 1983. The seismic inverse problem as a sequence of before stack migrations. Proc. Internat. Conf. "Inverse Scattering, Theory and Applications", Tulsa, OK. SIAM Publishers, Philadelphia.

Lambaré, G., 2008. Stereotomography. Geophysics, 73: VE25-VE34.

Lindsey, J.P., 1960. Elimination of seismic ghost reflections by means of a linear filter. Geophysics, 25: 130-140.

Liu, J. and Han, W., 2010. Automatic event picking and tomography on 3D RTM angle gathers. Expanded Abstr., 80th Ann. Internat. SEG Mtg., Denver: 4263-4268.

Liu, Z. and Bleistein, N., 1995. Migration velocity analysis: Theory and an iterative algorithm. Geophysics, 60: 142-153.

Luo, Y. and Schuster, G.T., 1991. Wave-equation traveltime inversion. Geophysics, 56: 645-653.

Ma, Y. and Hale, D., 2011. A projected Hessian matrix for full waveform inversion. Expanded Abstr., 81st Ann. Internat. SEG Mtg., San Antonio: 2401-2405.

Operto, S., Xu, S. and Lambaré, G., 2000. Can we quantitatively image complex structures with rays? Geophysics, 65: 1223-1238.

Plessix, R.-E., de Roeck, Y.H. and Chavent, G., 1999. Waveform inversion of reflection seismic data for kinematic parameters by local optimization. Siam J. on Scient. Comput., 20: 1033-1052.

Plessix, R.-E. and Rynja, H., 2010. VTI full waveform inversion: a parameterization study with a narrow azimuth streamer data example. Expanded Abstr., 80th Ann. Internat. SEG Mtg., Denver: 962-966.

Plessix, R.-E., Baeten, G., de Maag, J.W., Klaassen, M., Rujie, Z. and Zhifei, T., 2010. Application of acoustic full waveform inversion to a low-frequency large-offset land data set. Expanded Abstr., 80th Ann. Internat. SEG Mtg., Denver: 930-934.

Polyanin, A.D. and Manzhirov, A.V., 1998, Handbook of Integral Equations. CRC Press, Boca Raton, FL.

Pratt, R., Shin, C. and Hicks, G., 1998. Gauss-Newton and full Newton methods in frequency-space seismic waveform inversion. Geophys. J. Internat., 13: 341-362.

Ravaut, C., Operto, S., Improta, L., Virieux, J., Herrero, A. and Dell'Aversana, P., 2004. Multiscale imaging of complex structures from multifold wide-aperture seismic data by frequency-domain full waveform tomography: application to a thrust belt. Geophys. J. Internat., 159: 1032-1056.

Sava, P.C., Biondi, B. and Etgen, J., 2005. Wave-equation migration velocity analysis by focusing diffractions and reflections. Geophysics, 70: U19-U27.

Shen P. and Symes, W.W., 2008. Automatic velocity analysis via shot profile migration. Geophysics, 73: VE49-VE59.

Siliqi, R., Herrmann, P., Prescott, A. and Capar, L., 2007. High-order RMO picking using uncorrelated parameters. Expanded Abstr., 77th Ann. Internat. SEG Mtg., San Antonio: 2772-2776.

Sirgue, L., Pratt, R.G., 2004. Efficient waveform inversion and imaging: A strategy for selecting temporal frequencies. Geophysics, 69: 231-248.

Sirgue, L., Barkved, O.I., Dellinger, J., Etgen, J., Albertin, U. and Kommedal, J.H., 2010. Full-waveform inversion: the next leap forward in imaging at Valhall. First Break, 28: 65-70.

Soubaras, R. and Gratacos, B., 2007. Velocity model building by semblance maximization of modulated-shot gathers. Geophysics, 72: U67-U73.

Symes, W.W. and Carazzone, J.J., 1991. Velocity inversion by differential semblance optimization. Geophysics, 56: 654-663.

Tarantola, A., 1984. Inversion of seismic reflection data in the acoustic approximation. Geophysics, 49: 1259-1266.

Virieux, J. and Operto, S., 2009. An overview of full waveform inversion in exploration geophysics. Geophysics, 74(6): WCC127-WCC152.

Woodward, M.J., Nichols, D., Zdraveva, O., Whitfield, P. and Johns, T., 2008. A decade of tomography. Geophysics, 73(5): VE5-VE11.

Xu, S., Chauris, H., Lambaré, G. and Noble, M., 2001. Common angle migration: a strategy for imaging complex media. Geophysics, 66: 1877-1894.

Xu, S., Zhang, Y. and Tang, B., 2011. 3D angle gathers from reverse time migration. Geophysics, 76(2): S77-S92. doi: 10.1190/1.3536527

Zhang, S., Schuster, G. and Luo, Y., 2011. Wave-equation reflection traveltime inversion. Expanded Abstr., 81st Ann. Internat. SEG Mtg., San Antonio: 2705-2710.

Zhang, Y., Xu, S., Bleistein, N. and Zhang, G., 2007. True-amplitude, angle-domain, common-image gathers from one-way wave-equation migrations. Geophysics, 72: S49-S58.

Zhang, Y. and Wang, D., 2009. Traveltime information-based wave-equation inversion. Geophysics, 74(6): WCC27-WCC36.

Zhang, Y., Duan, L. and Roberts, G., 2013. True amplitude reverse time migration: from reflectivity to velocity and impedance perturbations. Extended Abstr., 75th EAGE Conf., London.

Zhou, H., Gray, S.H., Young, J., Pham, D. and Zhang, Y., 2003. Tomographic residual curvature analysis: The process and its components. Expanded Abstr., 73rd Ann. Internat. SEG Mtg., Dallas: 666-669.